Frequency Locking of an Optical Cavity Using a Time-Varying Kalman Filtering Approach

Sayed Z. Sayed Hassen, *Member, IEEE*, and Ian R. Petersen, *Fellow, IEEE*

***Abstract*— The cavity frequency locking problem, which arises in the field of quantum optics, involves matching the resonant frequency of an optical cavity to that of an incoming laser. Although this problem is investigated using linear control techniques for small perturbations, in this brief, we address the nonlinear control problem of frequency locking an optical cavity. Models of the measurement nonlinearities inherent in optical cavities are derived using a singular perturbation approach and instantaneous bounds are placed on the observation errors. A convex set within which the error between the laser frequency and the cavity resonant frequency lies is then determined at each time step by solving two high-order polynomial equations. Based on a reduced-order model of the cavity, a time-varying Kalman filter is designed and simulation results are presented to validate our controller on a full-model of the cavity in the nonlinear region of operation.**

***Index Terms*— Frequency locking, Kalman filtering, optical cavity.**

I. Introduction

ONE of the most promising applications of quantum optics is the interferometric gravity wave detector. The purpose of the gravitational wave detector is to detect perturbations in geometry which propagates through space like a wave as a result of a change in the mass distribution of objects. The size of the effect of a gravitational wave is given by a relative change in distance in the interferometer and it is usually of the order of a factor of 10^{-20} (depending on the type of astrophysical objects being considered); see [1], [2]. At this level of precision and sensitivity, gravitational waves are hard to detect and require lasers with extremely high levels of frequency stabilization.

Different approaches to the frequency stabilization of lasers are investigated and applied in the physics literature [3]–[6]. A prominent and widely used method for frequency stabilization is the Pound-Drever-Hall (PDH) approach [7], [8]. The PDH approach to frequency stabilization suppresses variations in the frequency of the laser by continuously comparing the laser's frequency with the resonant frequency of a fixed Fabry-Perot cavity [9]. Although this scheme works well when the laser frequency is close to the resonant frequency of the cavity, it breaks down when the difference between the two frequencies is large. In particular, the PDH approach becomes unreliable as the derivative of the reflected intensity goes to zero [10]. This issue also arises in other schemes, such as in [11] where the error signal was generated using homodyne detection [9]. In addition, it also happens that the error signal can be zero at frequencies other than the resonant frequency of the cavity, where there exists small linear regions of operation. Using linear control techniques will result in a cavity lock at frequencies other than the resonant frequency.

In this brief, we seek to address this problem by proposing a control approach that will frequency lock an optical cavity to a laser at its resonant frequency from any given initial operating point. A piezoelectric actuator is used to control the position of one of the cavity mirrors such that the natural frequency of the cavity is locked to the laser frequency. The cavity system is separated into two subsystems comprising of the mechanical part and the optical part. The time-scale of each subsystem being widely different with the dynamics of the optical cavity having a much smaller time constant, we use a singular perturbation approach [12] to model the optical cavity as a sensor nonlinearity. For measurement, we have two signals which are readily available; the phase quadrature of the cavity, which is measured using homodyne detection and the transmitted intensity (transmittance) measured with a photodiode. In this brief, we extended a preliminary conference version of this brief [13] by modeling the nonlinearities which arise in both the major and minor optical modes (high finesse and low finesse modes) of the optical cavity [10]. We allow for instantaneous bounded measurement noises in our observations and we determine the set of all frequency errors compatible with such observations at each time-step using Laguerre's method [14]. Information from this set is then used to update the parameters of a time-varying Kalman filter at each time instant. In this respect, the filtering problem is related to the deterministic interpretation of the Kalman filter as described in [15] where a set-membership description of the disturbance was used. It is also worthwhile mentioning that our control approach caters for slowly varying laser noise by including integral action in the controller design through the use of a variant of the integral linear quadratic Gaussian (LQG) approach proposed in [11]. The system is simulated under realistic conditions to show the performance of the nonlinear controller.

II. Background and Motivation

Side locking is probably the simplest modulation-free locking technique that is used to frequency lock optical cavities [16]. The technique relies on the system to be operating close to the resonant frequency of the laser such that small

Manuscript received August 31, 2012; revised May 26, 2013; accepted May 31, 2013. Manuscript received in final form June 4, 2013. Date of publication June 21, 2013; date of current version April 17, 2014. This work was supported in part by the Australian Research Council. Recommended by Associate Editor A. Serrani.

The authors are with the School of Electrical Engineering and Information Technology, University of New South Wales at the Australian Defence Force Academy, Canberra 2600, Australia (e-mail: sayed.hassen@gmail.com; i.r.petersen@gmail.com).

Color versions of one or more of the figures in this paper are available online at http://ieeexplore.ieee.org.

Digital Object Identifier 10.1109/TCST.2013.2266693

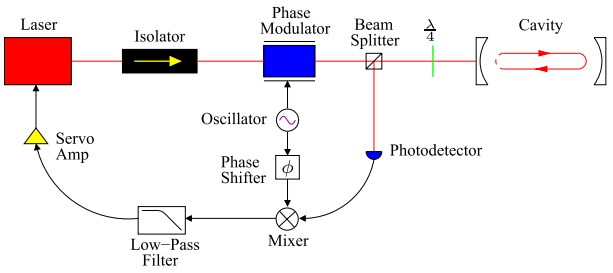

Fig. 1. Schematic layout of a PDH laser frequency locking control loop.

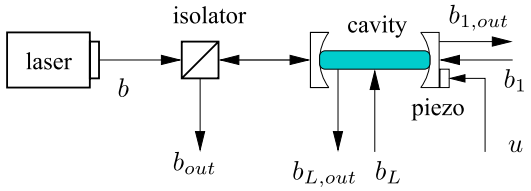

Fig. 2. Cavity locking feedback control loop.

deviations about this frequency causes proportional changes in the generated voltage used to drive the laser. The capture region usually extends up to about 2% of the free spectral range (FSR), beyond which the error signal becomes too noisy and control is also relatively slow using this technique. The FSR is defined as the difference between two adjacent resonant frequencies [9]

$$\text{FSR} = c/2L \text{ (Hz)}. \tag{1}$$

Here, c is the speed of light and $2L$ is the optical path length for one round trip through the cavity. In the case of a linear cavity, $L = nd$, where n is the refractive index of the material inside the cavity and d is the physical separation between the two mirrors. The need for fast control resulted in the development of the PDH technique, where the phase quadrature of the laser field is modulated. The phase is modulated much more rapidly than the characteristic time-scale of the optical cavity and hence the dynamics of the cavity mode remain unaffected by the modulation [9], [10] for more details. Small variations in the laser frequency away from the cavity resonance then convert the phase modulation of the laser field to amplitude modulation of the reflected field which is detected and demodulated. The basic layout used for PDH locking is as shown in Fig. 1.

In general, the controllers traditionally used to lock optical cavities in the physics community are the outcome of ad-hoc processes. We partially addressed this problem in [17] and [11] where an LQG controller was designed for an identified optical cavity system. The corresponding controlled system is experimentally tested and is found to be capable of handling small constant disturbances. We also showed that as long as the error signal is within a capture range, the detuning will be reduced and the system will come back into lock. The detuning refers to the difference between the laser frequency and the resonant frequency of the optical cavity and is denoted by Δ. However, the system would go out of lock and would remain out of lock if the applied disturbance pushed it outside the capture range. To resolve this problem, we propose a novel control algorithm that considers the nonlinearities present in the system and locks the laser cavity from *any* given initial operating point. The capture region is thus, enlarged to include the whole operating region.

III. Optical Cavity Locking Problem

One of the most well-known types of optical cavity is the Fabry-Perot cavity [19] which is formed by two partially transmitting mirrors facing each other and that are spaced apart by large distances compared with the size of the mirrors. The mirrors are curved in such a way that the desired optical modes (transverse modes) set up inside the cavity are well defined with smooth and regular transverse patterns [18]. The two waves traveling in the forward and reverse direction in a Fabry-Perot cavity set up an optical standing-wave which has a periodic spatial variation along the axis of the cavity with a period equal to one-half the optical wavelength. Depending on the length of the cavity, the plane waves propagating inside the cavity interact constructively resulting in stable optical modes and in a resonant mode, or destructively giving rise to unstable optical modes. The resonant frequency of an optical cavity depends upon its optical path length. The optical path length is usually modified by using a piezoelectric actuator attached to one of the mirrors of the cavity. In this way, the piezoelectric actuator adjusts the detuning variable Δ. Our aim is to frequency lock an optical cavity to a free running laser. The components in the cavity locking system are shown in Fig. 2.

The laser mode b of frequency ω_0 is modeled by a boson field $b = \beta + b_0$ where β is a real number (without loss of generality) and b_0 is a vacuum field, which is modeled as a standard quantum Gaussian white noise with unit variance [19]. The cavity is also coupled to two other optical fields: a transmitted mode b_1, and a loss mode b_L. A quadrature of the laser field reflected by the cavity b_{out} is measured using homodyne detection, producing a classical electrical signal y_1. The transmittance obtained from $b_{1,\text{out}}$, which represents the transmitted light intensity from the cavity is also measured as y_2.

IV. Modeling

The model of the cavity system being considered is made up of two parts: a mechanical subsystem representing the dynamics of the piezoelectric actuator, the controlled mirror and the power amplifier driving the actuator; and an optical subsystem representing the dynamics of the optical cavity. This partitioning of the overall system is necessary for modeling the nonlinearity of the system as we will see in the sequel. A block diagram of the cavity system is shown in Fig. 3. The control signal u together with a mechanical noise process w feeds into the mechanical subsystem generating the detuning Δ at its output. However, Δ is not directly available for measurement and instead we have the two measurement signals y_1 and y_2. The signal y_1 is measured using a standard homodyne detection method and includes a sensor noise v_1. Similarly, y_2 is measured using a photodiode and includes a sensor noise v_2. In addition, there are other noise sources

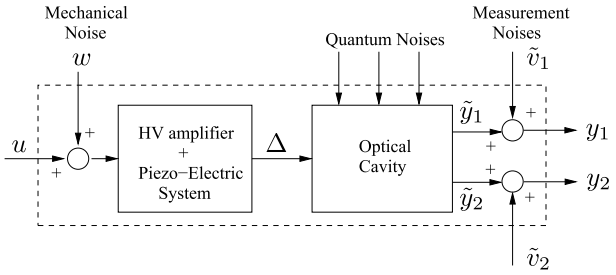

Fig. 3. Block diagram of the cavity system.

that enter the optical cavity which are referred to as quantum noises. These are discussed more detail in Section IV-B.

A. Optical Cavity

The cavity can be described in the Heisenberg picture by the following quantum stochastic differential equations [9], [19]:

$$\dot{a} = -(\frac{\kappa}{2} - i\,\Delta)a - \sqrt{\kappa}_0(\beta + b_0) - \sqrt{\kappa}_1 b_1 - \sqrt{\kappa}_L b_L$$
$$b_{\text{out}} = \sqrt{\kappa}_0 a + \beta + b_0 \tag{2}$$
$$b_{1,\text{out}} = \sqrt{\kappa}_1 a + b_1. \tag{3}$$

Here, the annihilation operator for the cavity mode is denoted by a and the annihilation operator for the coherent input mode is denoted by $b = \beta + b_0$, where b_0 is quantum noise. We write

$$\kappa = \kappa_0 + \kappa_1 + \kappa_L \tag{4}$$

where κ is the decay rate of the cavity and is usually measured in hertz (Hz). κ_0 quantifies the coupling strength of the field b_0 to the cavity. Similarly, κ_1 and κ_L quantify the strength of the couplings of the optical fields b_1 and b_L to the cavity, respectively. The measured signals are determined by the quantities

$$\begin{aligned}\tilde{y}_1 &= e^{-i\phi} b_{\text{out}} + e^{i\phi} b_{\text{out}}^\dagger \\ &= \sqrt{\kappa}_0(e^{-i\phi} a + e^{i\phi} a^\dagger) + 2\beta\cos\phi + q_0 \qquad (5)\\ \tilde{y}_2 &= b_{1,\text{out}}^\dagger b_{1,\text{out}} \\ &= \kappa_1 a^\dagger a + \sqrt{\kappa_1}(a^\dagger b_1 + b_1^\dagger a) + b_1^\dagger b_1 \qquad (6)\end{aligned}$$

where † is the conjugate transpose and $q_0 = e^{-i\phi} b_0 + e^{i\phi} b_0^\dagger$ is standard Gaussian white noise. In addition, the factor $e^{\pm i\phi}$ in (5) arises due to the interaction of the output field b_{out} with the homodyne detector as explained in Section IV-B.

B. Quadrature Measurement

We model the measurement of the X_ϕ quadrature of b_{out} via homodyne detection by changing the coupling operator for the laser mode to $\sqrt{\kappa}_0 e^{-i\phi} a$, and measuring the real quadrature of the resulting field. To this end, the cavity dynamics are reformulated in terms of the quadrature variables. We write

$$q = a + a^\dagger, \quad p = i(a^\dagger - a)$$

for the amplitude and phase quadratures, respectively. We can now express the cavity dynamics in state-space form as follows:

$$\begin{aligned}\begin{bmatrix}\dot{q}\\ \dot{p}\end{bmatrix} &= \begin{bmatrix}-\frac{\kappa}{2} & -\Delta\\ \Delta & -\frac{\kappa}{2}\end{bmatrix}\begin{bmatrix}q\\ p\end{bmatrix} - \begin{bmatrix}2\beta\sqrt{\kappa_0}\\ 0\end{bmatrix}\\ &\quad -\sqrt{\kappa}_0\begin{bmatrix}\cos\phi & \sin\phi\\ -\sin\phi & \cos\phi\end{bmatrix}\begin{bmatrix}q_0\\ p_0\end{bmatrix}\\ &\quad -\sqrt{\kappa}_1\begin{bmatrix}1 & 0\\ 0 & 1\end{bmatrix}\begin{bmatrix}q_1\\ p_1\end{bmatrix} - \sqrt{\kappa}_L\begin{bmatrix}1 & 0\\ 0 & 1\end{bmatrix}\begin{bmatrix}q_L\\ p_L\end{bmatrix}\\ y_1 &= k_2\sqrt{\kappa_0}\begin{bmatrix}\cos\phi & \sin\phi\end{bmatrix}\begin{bmatrix}q\\ p\end{bmatrix} + k_2\begin{bmatrix}1 & 0\end{bmatrix}\begin{bmatrix}q_0\\ p_0\end{bmatrix}\\ &\quad + 2k_2\beta\cos\phi + \tilde{v}_1 \qquad (7)\\ y_2 &= \tilde{k}_2\left(\frac{\kappa_1}{4}(p^2+q^2) + \frac{\sqrt{\kappa_1}}{2}\begin{bmatrix}q & p\end{bmatrix}\begin{bmatrix}q_1\\ p_1\end{bmatrix}\right) + \tilde{v}_2 \qquad (8)\end{aligned}$$

with noise quadratures $q_j = b_j + b_j^\dagger, p_j = i(p_j^\dagger - q_j)$, for $j = 0, 1, L$ (all standard Gaussian white noises). Here, y_1 is the output of the first sensor in which we have included the noise term $\tilde{v}_1$ and k_2 is the trans-impedance gain of the homodyne detector. Similarly, y_2 is the measurement of the transmitted light intensity which includes the sensor noise $\tilde{v}_2$ and $\tilde{k}_2$ is the sensor gain of the associated photodiode.

C. Separation of Time-Scale Approach to Nonlinearity Modeling

When the detuning variable Δ is treated as an input signal in (7), the system is nonlinear. Linear control design techniques can be applied to the system only when the variations of Δ about the operating point are small. In general, the detuning variable Δ may be large. In this section, we model the nonlinear behavior of the system in an effort to control the system for large values of Δ. Ignoring the noise terms q_0, p_0, q_1, p_1, q_L and p_L in (7), we can write

$$\dot{q} = -\frac{\kappa}{2}q - p\Delta - 2\sqrt{\kappa_0}\beta \tag{9}$$
$$\dot{p} = -\frac{\kappa}{2}p + q\Delta. \tag{10}$$

In most problems of interest, the optical cavity has a very large value of κ, implying that it has a large bandwidth and is a very fast system compared with the mechanical subsystem. This feature allows for a decomposition of the system via a separation of time-scales. The optical cavity can thus be modeled as a sensor nonlinearity applied to the variable Δ. The amplification provided then varies depending on the operating point. This approach to simplifying the system is known as the singular perturbation method [12].

To determine the characteristics of the static nonlinearity that approximates the fast subsystem, we set $\dot{q} = \dot{p} = 0$ in (9) and (10) and obtain the following:

$$\begin{aligned}\begin{bmatrix}q\\ p\end{bmatrix} &= \begin{bmatrix}-\frac{\kappa}{2} & -\Delta\\ \Delta & -\frac{\kappa}{2}\end{bmatrix}^{-1}\begin{bmatrix}2\sqrt{\kappa_0}\beta\\ 0\end{bmatrix}\\ &= \frac{-1}{(\frac{\kappa}{2})^2 + \Delta^2}\begin{bmatrix}\kappa\beta\sqrt{\kappa_0}\\ 2\beta\sqrt{\kappa_0}\Delta\end{bmatrix}. \qquad (11)\end{aligned}$$

For the case when $\phi = \frac{\pi}{2}$ in (7), the two measurements available can then be written as follows:

$$\begin{aligned} y_1 &= k_2\sqrt{\kappa_0}\,p + 2k_2\beta\cos\phi + v_1 \\ &= -\frac{2k_2\beta\kappa_0\Delta}{(\frac{\kappa}{2})^2+\Delta^2} + v_1 \quad (\text{since } \cos\phi = 0) \\ &= f_1(\Delta) + v_1 \end{aligned} \tag{12}$$

$$\begin{aligned} y_2 &= k_3(p^2+q^2) + v_2 = \frac{k_3\beta^2\kappa_0}{(\frac{\kappa}{2})^2+\Delta^2} + v_2 \\ &= f_2(\Delta) + v_2. \end{aligned} \tag{13}$$

Here, we have combined all the noise terms together such that

$$\begin{aligned} v_1 &= \tilde{v}_1 + k_2\, q_0 \\ v_2 &= \tilde{v}_2 + \frac{1}{2}\tilde{k}_2\sqrt{\kappa_1}\begin{bmatrix} q & p \end{bmatrix}\begin{bmatrix} q_1 \\ p_1 \end{bmatrix} \\ k_3 &= \frac{1}{4}\tilde{k}_2\kappa_1. \end{aligned}$$

Note that the quantity ϕ can be chosen by changing the orientation of the quarter-wave/half-wave plate along the beam path. In addition, the term $2k_2\beta\cos\phi$ adds a constant component to the measurement y_1. The equations derived for the two measurement signals (12) and (13) are applicable in the presence of a single optical mode, which in our case is chosen as the low finesse mode of the optical cavity. In practice, there are higher order modes of the optical cavity which introduce additional nonlinearities. In particular, the second-order optical mode (which we will refer to as the high finesse mode) is large enough to warrant its consideration when determining the measured signals. The shape of the nonlinearity for the high finesse mode is exactly the same as determined for the low finesse mode and differs only in magnitude and sign. It is also symmetric about the low finesse mode. For a more complete description, the measurement signals as described by (12) and (13) are modified to include the high finesse mode as follows:

$$\begin{aligned} y_1 = &-\frac{2k_2\beta\kappa_0\Delta}{(\frac{\kappa}{2})^2+\Delta^2} + \frac{2\alpha_1 k_2\beta\kappa_0(\Delta+\gamma)}{(\frac{\kappa}{2})^2+(\Delta+\gamma)^2} \\ &+\frac{2\alpha_1 k_2\beta\kappa_0(\Delta-\gamma)}{(\frac{\kappa}{2})^2+(\Delta-\gamma)^2} + v_1 \end{aligned} \tag{14}$$

$$\begin{aligned} y_2 = &\frac{k_3\beta^2\kappa_0}{(\frac{\kappa}{2})^2+\Delta^2} + \frac{\alpha_2 k_3\beta^2\kappa_0}{(\frac{\kappa}{2})^2+(\Delta+\gamma)^2} \\ &+\frac{\alpha_2 k_3\beta^2\kappa_0}{(\frac{\kappa}{2})^2+(\Delta-\gamma)^2} + v_2. \end{aligned} \tag{15}$$

Here, the quantities $\alpha_{1,2}$ represent scaling factors on the gain of the high finesse mode and γ represents the frequency difference between the low finesse and high finesse resonant frequencies. Using typical values for the parameters in an experimental optical cavity system (Table I), the plots shown in Fig. 4 are generated to show the effect of the detuning variable Δ on the measurement signals y_1 and y_2. It is clear that maximum transmission occurs when the detuning variable Δ approaches zero. This occurs when the frequency of the laser is equal to the cavity's FSR.

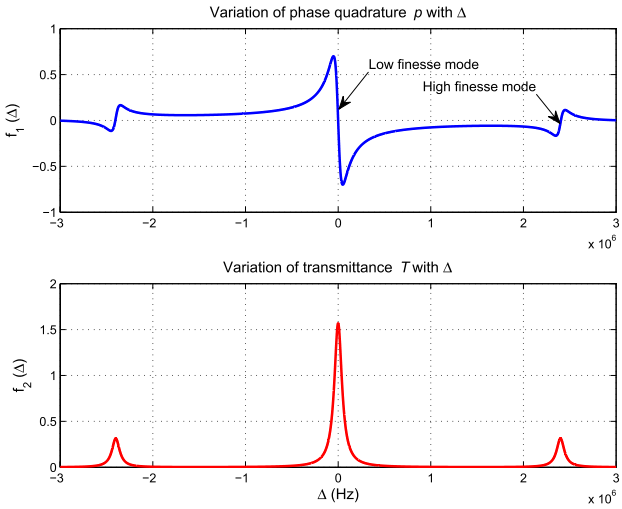

Fig. 4. Variation of functions $f_1(\Delta)$ and $f_2(\Delta)$ with Δ.

The curves shown in Fig. 4 correspond to the characteristic curves that would be obtained if the cavity length is scanned using a piezoelectric transducer attached to one of the cavity mirrors; see [5], [20]. In addition, in practice, this feature is repeated at integer multiples of the cavity's FSR. We will take advantage of the periodic nature of the system in designing our controller.

D. Piezoelectric Actuator and Mirror Mount Model

A typical model is used to represent the piezoelectric actuator and mirror mount of the system. Indeed, for the purpose of controller design, it suffices to consider a model which is a simple second-order system with a resonant mode. We choose the resonant frequency at 8.5 krad/s which is typical for actuators used for this purpose. However, for simulation purposes, we will use a higher order model, which includes additional resonant modes. The second-order model is discretized at a sampling frequency of 20 kHz and the resulting discrete-time state-space plant model is of the form

$$x_{k+1} = Ax_k + Bu_k \qquad \Delta_k = Cx_k \tag{16}$$

where $A \in \mathbf{R}^2$, $B \in \mathbf{R}^{2\times 1}$ and $C \in \mathbf{R}^{1\times 2}$. Here, Δ is measured in hertz (Hz) and the control signal u has units of volts (V).

V. Main Result

As shown in [11], using only the measurement y_1, it was possible to attenuate the different sources of noise affecting the system provided that the system is operating close to the linear region, which happens only for small values of Δ. If the system is perturbed strongly enough (which is often the case in practice) and goes far enough outside the linear operating region, it becomes effectively unobservable (with only y_1 as measurement). Outside of the linear region, the effective sensor gain may also change sign tending to drive the system away from resonance. We seek to construct a control law that would overcome this problem and that would be capable of taking the system from the nonlinear region back to the linear region.

Using both measurements y_1 and y_2 to control the cavity system may at first sight seem to provide a trivial solution to the problem. However, both measurement signals tend to zero for large values of $|\Delta|$, and in the presence of measurement noises, the system then becomes extremely sensitive to measurement errors. We next propose a systematic approach to estimate the state of the nonlinear dynamical system using noise corrupted measurements when the measurement noise is assumed to be unknown but bounded.

A. Bounded Noise Model

A model of the measurement noise is considered involving instantaneous constraints on the noise variables v_1 and v_2 in (12) and (13), respectively. We bound the measurement errors v_{1_k} and v_{2_k} at each instant of time k; i.e.,

$$v_{1_k}^2 \le \mu_1^2; \qquad v_{2_k}^2 \le \mu_2^2 \tag{17}$$

where μ_1 and μ_2 are the fixed constants denoting the magnitude of the noise. If we allow

$$y_{1_k} = f_1(\Delta_k) + v_{1_k} \qquad y_{2_k} = f_2(\Delta_k) + v_{2_k}$$

where

$$f_1(\Delta_k) = \frac{-2k_2\beta\kappa_0\Delta_k}{(\frac{\kappa}{2})^2 + \Delta_k^2} + \frac{2\alpha_1 k_2\beta\kappa_0(\Delta_k + \gamma)}{(\frac{\kappa}{2})^2 + (\Delta_k + \gamma)^2} + \frac{2\alpha_1 k_2\beta\kappa_0(\Delta_k - \gamma)}{(\frac{\kappa}{2})^2 + (\Delta_k - \gamma)^2} \tag{18}$$

$$f_2(\Delta_k) = \frac{k_3\beta^2\kappa_0}{(\frac{\kappa}{2})^2 + \Delta_k^2} + \frac{\alpha_2 k_3\beta^2\kappa_0}{(\frac{\kappa}{2})^2 + (\Delta_k + \gamma)^2} + \frac{\alpha_2 k_3\beta^2\kappa_0}{(\frac{\kappa}{2})^2 + (\Delta_k - \gamma)^2} \tag{19}$$

we then consider the problem of characterizing the set of all possible Δ_k compatible with the given observations y_{1_k} and y_{2_k}; i.e., to find the set

$$\mathcal{S} = \Big\{\Delta_k \in \mathbb{R} : (y_{1_k} - f_1(\Delta_k))^2 \le \mu_1^2 \text{ and } (y_{2_k} - f_2(\Delta_k))^2 \le \mu_2^2\Big\}. \tag{20}$$

It is then straightforward to verify that the set $\mathcal{S}$ is equal to the set of $\Delta_k \in \mathbb{R}$ satisfying the following two inequalities:

$$a_{12}\Delta_k^{12} + a_{11}\Delta_k^{11} + \cdots + a_1\Delta_k + a_0 \le 0 \tag{21}$$

$$b_{12}\Delta_k^{12} + b_{11}\Delta_k^{11} + \cdots + b_1\Delta_k + b_0 \le 0 \tag{22}$$

where $a_0, a_1, \cdots, a_{12}$, and $b_0, b_1, \cdots, b_{12}$ are defined in the Appendix. The set $\mathcal{S}$ is constructed by first equating the left-hand side of the inequalities (21) and (22) to zero and solving for the roots of the resulting two 12th order polynomials. We solve for these roots using Laguerre's method, which is by far the most straightforward method for solving high-order polynomials and it requires only a few iterations to obtain roots with high accuracy. This particular feature of the method makes it especially appealing for our application compared with other sure-fire methods; see also [21], [22].

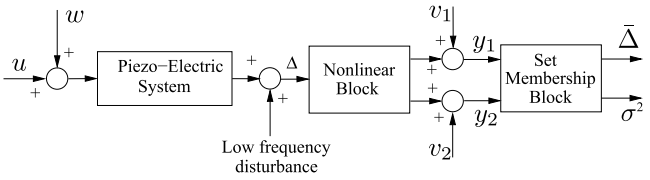

Fig. 5. Complete system model.

If we obtain m roots, after applying Laguerre's method, for $\Delta_{k,i}$ for $i = 1, \cdots, m$, these roots bound $m+1$ corresponding regions of interest which can be defined as follows:

$$\mathcal{S}_1 = \{\Delta_k \in \mathbb{R} : -\infty < \Delta_k < \Delta_{k,1}\}$$
$$\mathcal{S}_2 = \{\Delta_k \in \mathbb{R} : \Delta_{k,1} < \Delta_k < \Delta_{k,2}\}$$
$$\vdots$$
$$\mathcal{S}_{m+1} = \{\Delta_k \in \mathbb{R} : \Delta_{k,m} < \Delta_k < \infty\}.$$

The union of the sets $\mathcal{S}_i$, which have a point satisfying (21) and (22), defines the set $\mathcal{S}$. It is possible that the set $\mathcal{S}$ is nonconvex when the system is operating far from resonance. In those cases, we may end up with two regions on either side of the main resonant peak where the inequalities are satisfied. We then consider the convex hull of the set $\mathcal{S}$.

Given the set conv $\mathcal{S}_k$ at time step k, the corresponding mean and standard deviation are determined as follows (assuming a uniform probability distribution on conv $\mathcal{S}$):

$$\bar{\Delta} = \frac{1}{2}\left[\min_{\Delta\in\mathcal{S}_k}(\Delta) + \max_{\Delta\in\mathcal{S}_k}(\Delta)\right]$$
$$\sigma = \frac{1}{2\sqrt{3}}\left[\max_{\Delta\in\mathcal{S}_k}(\Delta) - \min_{\Delta\in\mathcal{S}_k}(\Delta)\right].$$

These quantities are then used to update the inputs of a discrete-time Kalman filter, where they define the new measurement Δ_k and the measurement covariance σ_k^2, respectively. This process is described in the next section.

VI. LQG Controller Design

The complete nonlinear model of the system as used for the controller design purpose is shown in Fig. 5. The state of a time-varying Kalman filter is updated using the new measurement $\bar{\Delta}_k$ and the variance σ_k^2 available at each instant of time. In this way, the nonlinear problem becomes one which fits into the standard framework of the LQG controller design.

A. LQG Cost Criterion and Integral Action

The LQG controller consists of an estimation block defined by a Kalman filter followed by a deterministic linear quadratic regulator state feedback gain. The regulator assumes that the estimate of the states are the actual states and determines the optimal control law corresponding to a given performance criterion. The system is also subjected to laser phase noise ($1/f^2$ noise) which in practice appears in the form of a slowly varying disturbance. A standard LQG controller is not able to drive the detuning variable Δ to zero in the face of such a disturbance. To regulate the detuning variable, we require integral action which is obtained by introducing an integrator

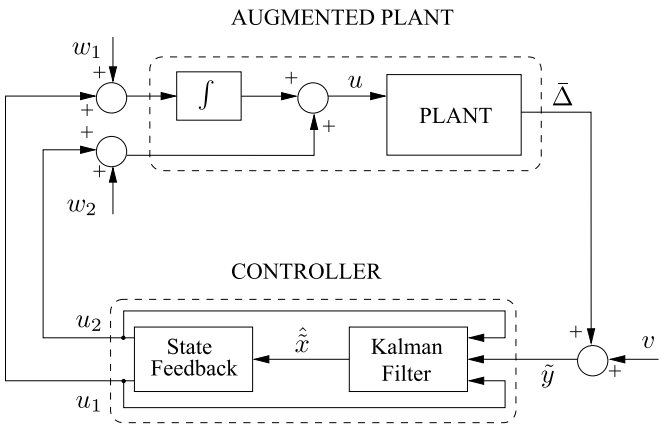

Fig. 6. Integral LQG controller design configuration.

at the output of the controller and by splitting the control signal u into two signals u_1 and u_2. These two signals are then generated by the controller. The plant, as seen by the controller is then the augmented plant as shown in Fig. 6. Before the LQG controller, as designed for the augmented plant is implemented, its output is appropriately augmented with the integrator to form the integral LQG controller. A fictitious process noise w_1 is included to ensure that the designed controller is such that suitable bandwidth and robustness are achieved. The measurement noise v is also included to model the variance of the detuning variable $\bar{\Delta}$.

A discretised augmented system, which we will use for controller design, can then be described as follows:

$$\begin{aligned} \tilde{x}_{k+1} &= \tilde{A}\tilde{x}_k + \begin{bmatrix} \tilde{B}_1 & \tilde{B}_2 \end{bmatrix} \begin{bmatrix} u_{1,k} \\ u_{2,k} \end{bmatrix} + \begin{bmatrix} \tilde{B}_1 & \tilde{B}_2 \end{bmatrix} \begin{bmatrix} w_{1,k} \\ w_{2,k} \end{bmatrix} \\ \tilde{y} &= \tilde{C}\tilde{x}_k + v_k \end{aligned} \tag{23}$$

where the mechanical noises $w_{i,k}$ for $i = 1, 2$, are assumed to be Gaussian white noises with variances ϵ_1^2 and ϵ_2^2, respectively. $\tilde{A}$, $\tilde{B} = [\tilde{B}_1 \ \ \tilde{B}_2]$, $\tilde{C}$ represent the state, input and output matrices of the augmented system, respectively. The measurement noise v_k is assumed to be Gaussian white noise with variance σ_k^2. We also assume that the initial state x_0 is unknown but that $x_0 \sim N(\bar{x}_0, P_{x_0})$.

An LQG performance criterion is chosen so that the controller minimizes the detuning variable Δ while at the same time restricting the size of the control signal. This requirement is reflected in the following quadratic cost functional:

$$\mathcal{J} = \lim_{k\to\infty} \mathbf{E}\left[\sum_{k=1}^{\infty} (\tilde{x}_k^T Q \tilde{x}_k + u_k^T R u_k)\right]. \tag{24}$$

The matrices Q and R are chosen such that

$$\tilde{x}_k^T Q \tilde{x}_k = |\tilde{y}_k|^2 \quad u_k^T R u_k = r_1 |u_{1,k}|^2 + r_2 |u_{2,k}|^2 \tag{25}$$

where $r_1, r_2 > 0$ are treated as design parameters. The expectation in (24) is with respect to the Gaussian white noise present in the system. The optimal control is given by (e.g., [23], [24])

$$u_k = -F\hat{\tilde{x}}_k \tag{26}$$

where $\hat{\tilde{x}}$ is the state estimate, and

$$F = (\tilde{B}^T S \tilde{B} + R)^{-1} \tilde{B}^T S \tilde{A} \tag{27}$$

with S satisfying the following algebraic Riccati equation:

$$0 = \tilde{A}^T [S - S\tilde{B}(\tilde{B}^T S \tilde{B} + R)^{-1} \tilde{B} S] \tilde{A} - S + Q. \tag{28}$$

B. Discrete-Time Kalman Filtering

We now turn our attention to the estimation of the states $\hat{\tilde{x}}$ of the system on the basis of model (23). If the *a posteriori* estimate and error covariance are given by $\hat{\tilde{x}}_k$ and P_k, respectively, and $\hat{\tilde{x}}_k^-$, P_k^- are the respective *a priori* quantities, then the state of the system is estimated recursively using the following Kalman filter equations (e.g., [25], [26]):

$$K_k = P_k^- \tilde{C}^T (\tilde{C} P_k^- \tilde{C}^T + \sigma_k)^{-1}, \quad P_0^- = P_{\tilde{x}_0} \tag{29}$$

$$\hat{\tilde{x}}_k = \hat{\tilde{x}}_k^- + K_k(\tilde{y}_k - \tilde{C}\hat{\tilde{x}}_k^-), \quad \hat{\tilde{x}}_0^- = \bar{\tilde{x}}_0 \tag{30}$$

$$P_k = (I - K_k \tilde{C}) P_k^- \tag{31}$$

and

$$\begin{aligned} \hat{\tilde{x}}_{k+1}^- &= \tilde{A}\hat{\tilde{x}}_k + \tilde{B}u_k \\ P_{k+1}^- &= \tilde{A} P_k \tilde{A}^T + \tilde{B} W \tilde{B}^T \end{aligned} \tag{32}$$

where

$$W = \begin{bmatrix} \epsilon_1 & 0 \\ 0 & \epsilon_2 \end{bmatrix}.$$

At each time instant, the new measurement $\tilde{y}_k = \bar{\Delta}_k$ and measurement covariance σ_k are determined from the set $\mathcal{S}$ in (20) and are used to update $\hat{\tilde{x}}_k$ in (30) and P_k using (31) and (29). In designing the LQG controller, the following parameters are chosen for good controller performance. The process noise variances are chosen to be $\epsilon_1 = 1 \times 10^4$ and $\epsilon_2 = 0.1$, respectively, and the control weights are set at $r_1 = 3 \times 10^8$ and $r_2 = 3 \times 10^{15}$.

VII. Simulation

To reflect the true behavior of the electromechanical system, we simulate the controller with the linear part of the plant being replaced by a sixth-order model. This new model includes higher order resonant modes at frequencies of 15 and 30 krad/s, as could be expected from a typical piezo-electric actuator. The linear part of the plant used for simulation is thus given by the following:

$$\begin{aligned} G(s) = &\frac{3.38e7}{s^2 + 742.9s + 7.19e7} + \frac{7.5e6}{s^2 + 600s + 2.25e8} \\ &+ \frac{3e7}{s^2 + 600s + 9e8}. \end{aligned} \tag{33}$$

A comparison of the two models used for controller design and closed-loop simulation is shown in Fig. 7.

We simulate the system with the given control law (26) for a time period of 0.5 s and at a sampling rate of 20 kHz. The simulation parameters used for the model are the same as used previously in Table I and the noise bounds are chosen to reflect typical experimental conditions.

The system is initialized well outside the linear region beyond the high finesse mode, with $\Delta = 5 \times 10^6$ Hz

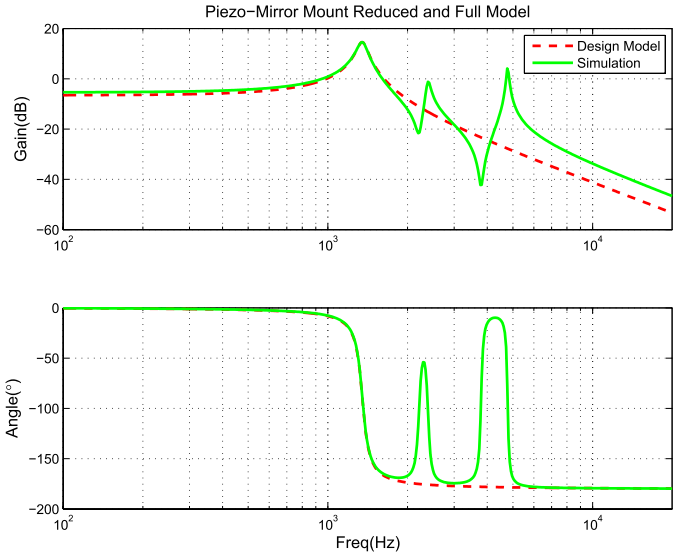

Fig. 7. Frequency response of design and simulation models.

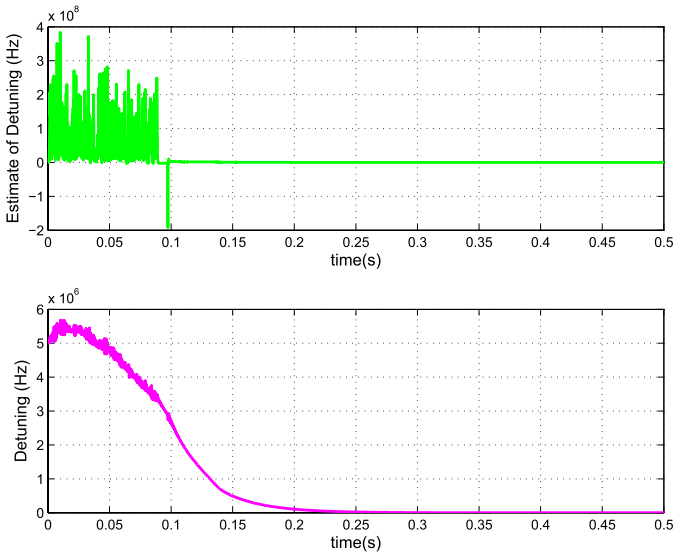

Fig. 9. Estimated and actual detuning variable Δ.

TABLE I
SIMULATION PARAMETER VALUES

Simulation parameters	Value	Simulation parameters	Value
β	7×10^7	k_3	8×10^{-9}
κ	1×10^5	$\alpha_{1,2}$	2×10^{-1}
κ_0	1×10^4	γ	2.4×10^6
k_2	5×10^{-8}	$\mu_{1,2}$	1×10^{-2}

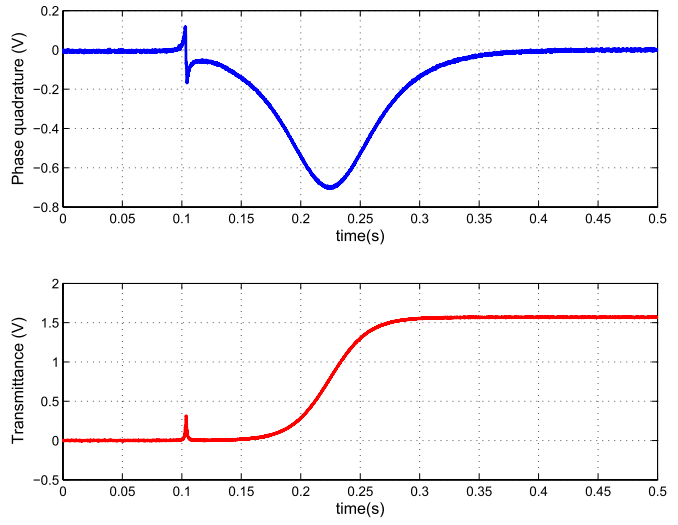

Fig. 8. Variation of the phase quadrature and transmittance.

(representing a constant dc disturbance) and white noises of suitable magnitude satisfying the design requirements (17) are included in the two measurement signals. The variation of the two measurement signals y_1 and y_2 corresponding to the phase quadrature p (V) and the transmittance I (V), respectively, are shown in Fig. 8. The measured signal y_1 is highly sensitive to small variations in Δ. The transmittance I settles at its peak value after about 0.35 s. The response of the true Δ as well as the estimated $\hat{\Delta}$ obtained from the time-varying Kalman filter is shown in Fig. 9. As expected, the estimated $\hat{\Delta}$ is very noisy at the start of the simulation given the effect of sensor noises on the set $\mathcal{S}$ when the system is far from resonance and when both y_1 and y_2 are initially zero. Simulation results on a high-order plant with additional resonant modes show that the controller is clearly effective in transferring the system from the nonlinear region into the linear region and regulates Δ close to zero.

VIII. CONCLUSION

We addressed the problem of stabilizing a nonlinear optical cavity system which arised in the field of experimental quantum optics. Taking advantage of the different time-scales of the interconnected systems, the mechanical subsystem comprised of a high-voltage amplifier, the PZT and the mirror mount were modeled separately from the faster dynamics associated with the optical cavity. Instantaneous error bounds were placed on the measurement noises and a convex set $\mathcal{S}$ of all frequency errors Δ consistent with the output measurements was determined by solving two high-order polynomial equations using Laguerre's method. A time-varying Kalman filter was then designed based on a second-order model for the mechanical subsystem dynamics. The presence of laser phase noise which acts like a slowly varying disturbance on the system was considered by augmenting the mechanical subsystem with an integrator prior to the filter design stage. Information from the convex set $\mathcal{S}$ was used to update the estimate of the states and the nonlinear problem was treated as an integral LQG control problem with a time-varying Kalman filter. Simulation results on a higher order model of the electromechanical system with an additional resonant modes showed that the controller was successful in regulating the detuning variable Δ in the presence of large constant/slowly varying disturbances and realistic noise models. Future research will involve validating our design in an experimental laboratory setting.

APPENDIX

COEFFICIENTS OF POLYNOMIALS

In this appendix, $a_0, a_1, \ldots, a_{12}$, and $b_0, b_1, \ldots, b_{12}$ stated in (21) and (22) are defined in detail.

$$
\begin{aligned}
a_{12} &= 4096(y_1^2 - \mu_1^2)\\
a_{11} &= -6144\beta_1 y_1/5\\
a_{10} &= 2304\beta_1^2/25 - (16384\gamma^2 - 6144\kappa^2)(y_1^2 - \mu_1^2)\\
a_9 &= 512\beta_1 y_1(56\gamma^2 - 15\kappa^2)/5\\
a_8 &= -\beta_1^2(12288\gamma^2 - 2304\kappa^2)/25\\
&\quad +(24576\gamma^4 - 12288\gamma^2\kappa^2 + 3840\kappa^4)(y_1^2 - \mu_1^2)\\
a_7 &= -768\beta_1 y_1(64\gamma^4 - 16\gamma^2\kappa^2 + 5\kappa^4)/5\\
a_6 &= \beta_1^2(24064\gamma^4 - 1536\gamma^2\kappa^2 + 864\kappa^4)/25\\
&\quad -(16384\gamma^6 - 8192\gamma^4\kappa^2 + 2048\gamma^2\kappa^4 - 1280\kappa^6)\\
&\quad \times(y_1^2 - \mu_1^2)\\
a_5 &= -192\beta_1 y_1(-192\gamma^6 + 8\gamma^2\kappa^4 + 5\kappa^6)/5\\
a_4 &= -\beta_1^2(20480\gamma^6 + 8448\gamma^4\kappa^2 - 1536\gamma^2\kappa^4 - 144\kappa^6)/25\\
&\quad +(4096\gamma^8 - 4096\gamma^6\kappa^2 + 1024\gamma^4\kappa^4\\
&\qquad +512\gamma^2\kappa^6 + 240\kappa^8)(y_1^2 - \mu_1^2)\\
a_3 &= -8\beta_1 y_1(1280\gamma^8 + 256\gamma^6\kappa^2 + 128\gamma^4\kappa^4\\
&\qquad +160\gamma^2\kappa^6 + 15\kappa^8)/5\\
a_2 &= \beta_1^2(6400\gamma^8 + 7680\gamma^6\kappa^2 + 2784\gamma^4\kappa^4\\
&\qquad +288\gamma^2\kappa^6 + 9\kappa^8)/25\\
&\quad +(2048\gamma^8\kappa^2 + 1024\gamma^6\kappa^4 + 512\gamma^4\kappa^6\\
&\qquad +192\gamma^2\kappa^8 + 24\kappa^{10})(y_1^2 - \mu_1^2)\\
a_1 &= -2\beta_1\kappa^2 y_1(4\gamma^2 + \kappa^2)^2(80\gamma^4 + 48\gamma^2\kappa^2 + 3\kappa^4)/5\\
a_0 &= \kappa^4(4\gamma^2 + \kappa^2)^4(y_1^2 - \mu_1^2).\\
b_{12} &= 4096(y_2^2 - \mu_2^2)\\
b_{11} &= b_9 = b_7 = b_5 = b_3 = b_1 = 0\\
b_{10} &= -14336\beta_2 y_2/5 - (16384\gamma^2 - 6144\kappa^2)(y_2^2 - \mu_2^2)\\
b_8 &= 12544\beta_2^2/25 + 45056\beta_2\gamma^2 y_2/5 - 3584\beta_2\kappa^2 y_2\\
&\quad +(24576\gamma^4 - 12288\gamma^2\kappa^2 + 3840\kappa^4)(y_2^2 - \mu_2^2)\\
b_6 &= -\beta_2^2(28672\gamma^2 - 12544\kappa^2)/25\\
&\quad -\beta_2 y_2(57344\gamma^4/5 - 4096\gamma^2\kappa^2 + 1792\kappa^4)\\
&\quad -(16384\gamma^6 - 8192\gamma^4\kappa^2 + 2048\gamma^2\kappa^4 - 1280\kappa^6)\\
&\quad \times(y_2^2 - \mu_2^2)\\
b_4 &= \beta_2^2(34304\gamma^4 - 3584\gamma^2\kappa^2 + 4704\kappa^4)/25\\
&\quad +\beta_2 y_2(36864\gamma^6 - 6144\gamma^4\kappa^2 - 1536\gamma^2\kappa^4 - 2240\kappa^6)/5\\
&\quad +(4096\gamma^8 - 4096\gamma^6\kappa^2 + 1024\gamma^4\kappa^4 + 512\gamma^2\kappa^6 + 240\kappa^8)\\
&\quad \times(y_2^2 - \mu_2^2)\\
b_2 &= \mu_2^2\Big[256\gamma^2\kappa^4(4\gamma^2 + \kappa^2)^2 - \kappa^4(4\gamma^2 + \kappa^2)^2(96\gamma^2 + 8\kappa^2)\\
&\qquad -(\kappa^4(96\gamma^2 + 8\kappa^2) + 8\kappa^2(4\gamma^2 + \kappa^2)^2)(4\gamma^2 + \kappa^2)^2\Big]\\
&\quad -2[(\beta_2 - \kappa^2 y_2)(4\gamma^2 + \kappa^2)^2 + 2\beta_2\kappa^2(4\gamma^2 + \kappa^2)/5]\\
&\quad \times\Big[y2\Big((4\gamma^2 + \kappa^2)(16\gamma^2 + 8\kappa^2)\\
&\qquad +4\kappa^2(4\gamma^2 + \kappa^2) - 64\gamma^2\kappa^2\Big)\\
&\qquad -2\beta_2(16\gamma^2 + 8\kappa^2)/5 + \beta_2(32\gamma^2 - 8\kappa^2)\Big]\\
b_0 &= [\beta_2(4\gamma^2 + \kappa^2)^2 - \kappa^2 y_2(4\gamma^2 + \kappa^2)^2\\
&\qquad +2\beta_2\kappa^2(4\gamma^2 + \kappa^2)/5]^2 - \mu_2^2\kappa^4(4\gamma^2 + \kappa^2)^4.
\end{aligned}
$$

REFERENCES

[1] P. Aufmuth and K. Danzmann, "Gravitational wave detectors," *New J. Phys.*, vol. 7, no. 202, pp. 1–3, Sep. 2005.

[2] J. Lu, D. G. Blair, and C. Zhao, "Detection of gravitational waves," *Rep. Prog. Phys.*, vol. 63, no. 9, pp. 1317–1427, 2000.

[3] A. D. White, "Frequency stabilization of gas lasers," *IEEE J. Quantum Elec.*, vol. 1, no. 8, pp. 349–357, Nov. 1965.

[4] R. L. Barger, M. S. Sorem, and J. L. Hall, "Frequency stabilization of a CW dye laser," *Appl. Phys. Lett.*, vol. 22, no. 11, pp. 573–575, 1973.

[5] T. W. Hansch and B. Couillaud, "Laser frequency stabilization by polarization spectroscopy of a reflecting reference cavity," *Opt. Commun.*, vol. 35, no. 3, pp. 441–444, Dec. 1980.

[6] C. E. Wieman and S. L. Gilbert, "Laser-frequency stabilization using mode interference from a reflecting reference interferometer," *Opt. Lett.*, vol. 7, no. 10,pp. 480–482, 1982.

[7] R. V. Pound, "Electronic frequency stabilization of microwave oscillators," *Rev. Sci. Instrum.*, vol. 17, no. 11, pp. 490–505, 1946.

[8] R. W. P. Drever, J. L. Hall, F. V. Kowalski, J. Hough, G. M. Ford, A. J. Munley, and H. Ward, "Laser phase and frequency stabilization using an optical resonator," *Appl. Phys. B*, vol. 31, no. 2, pp. 97–105, 1983.

[9] H. A. Bachor and T. C. Ralph, *A Guide to Experiments in Quantum Optics*. New York, NY, USA: Wiley, 2004.

[10] E. D. Black, "An introduction to Pound-Drever-Hall laser frequency stabilization," *Amer. J. Phys.*, vol. 69, no. 1, pp. 79–87, 2001.

[11] S. Z. Sayed Hassen, M. Heurs, E. H. Huntington, I. R. Petersen, and M. R. James, "Frequency locking of an optical cavity using linear-quadratic gaussian integral control," *J. Phys. B, Atmosph. Molecular Opt. Phys.*, vol. 42, no. 17, p. 175501, Sep. 2009.

[12] P. Kokotović, H. K. Khalil, and J. O'Reilly, *Singular Perturbation Methods in Control: Analysis and Design*. San Diego, CA, USA: Academic Press Inc., 1986.

[13] S. Z. Sayed Hassen and I. R. Petersen, "A time-varying Kalman filter approach to integral LQG frequency locking of an optical cavity," in *Proc. Amer. Control Conf.*, Jul. 2010, pp. 2736–2741.

[14] W. H. Press, S. A. Teukolsky, W. T. Vetterling, and B. P. Flannery, *Numerical Recipes: The Art of Scientific Computing*, 3rd ed. New York, NY, USA: Cambridge Univ. Press, 2007.

[15] D. P. Bertsekas and I. B. Rhodes, "Recursive state estimation for a set-membership description of uncertainty," *IEEE Trans. Autom. Control*, vol. 16, no. 2, pp. 117–128, Apr. 1971.

[16] K. B. MacAdam, A. Steinbach, and C. Wieman, "A narrow-band tunable diode laser system with grating feedback, and a saturated absorption spectrometer for Cs and Rb," *Amer. J. Phys.*, vol. 60, no. 12, pp. 1098–1111, Dec. 1992.

[17] S. Z. Sayed Hassen, E. Huntington, I. R. Petersen, and M. R. James, "Frequency locking of an optical cavity using LQG Integral Control," in *Proc. 17th IFAC World Congr.*, Jul. 2008, pp. 1821–1826.

[18] A. E. Siegman, *Lasers*. Mill Valley, CA, USA: University Science Books, 1986.

[19] C. W. Gardiner and P. Zoller, *Quantum Noise*. New York, NY, USA: Springer-Verlag, 2000.

[20] D. A. Shaddock, M. B. Gray, and D. E. McClelland, "Frequency locking a laser to an optical cavity by use of spatial mode interference," *Opt. Lett.*, vol. 24, no. 21, pp. 1499–1501, Nov. 1999.

[21] F. S. Acton, *Numerical Methods That Work*. New York, NY, USA: Harper & Row Publishers, 1990.

[22] S. Goedecker, "Remark on algorithms to find roots of polynomials," *SIAM J. Sci. Comput.*, vol. 15, no. 5, pp. 1059–1063, Sep. 1994.

[23] P. J. Antsaklis and A. N. Michel, *A Linear Systems Primer*. Cambridge, MA, USA: Birkhaüser, 2007.

[24] H. Kwakernaak and R. Sivan, *Linear Optimal Control Systems*. New York, NY, USA: Wiley, 1972.

[25] R. G. Brown, *Introduction to Random Signal Analysis and Kalman Filtering.* New York, NY, USA: Wiley, 1983.

[26] F. L. Lewis, *Optimal Estimation*. New York, NY, USA: Wiley, 1986.